SHORT COMMUNICATION

Journal of Semiconductors
(2021) 42, 050501
doi: 10.1088/1674-4926/42/5/050501

Efficient and photostable $CsPbI_2Br$ solar cells realized by adding PMMA

Yanbo Shang[1, ‡], Zhimin Fang[1, 2, ‡], Wanpei Hu[1], Chuantian Zuo[2], Bairu Li[1], Xingcheng Li[1], Mingtai Wang[3], Liming Ding[2, †], and Shangfeng Yang[1, †]

[1]Hefei National Laboratory for Physical Sciences at Microscale, Key Laboratory of Materials for Energy Conversion (CAS), Anhui Laboratory of Advanced Photon Science and Technology, Department of Materials Science and Engineering, University of Science and Technology of China, Hefei 230026, China

[2]Center for Excellence in Nanoscience (CAS), Key Laboratory of Nanosystem and Hierarchical Fabrication (CAS), National Center for Nanoscience and Technology, Beijing 100190, China

[3]Institute of Solid State Physics, Chinese Academy of Sciences, Hefei 230031, China

Citation: Y B Shang, Z M Fang, W P Hu, C T Zuo, B R Li, X C Li, M T Wang, L M Ding, and S F Yang, Efficient and photostable $CsPbI_2Br$ solar cells realized by adding PMMA[J]. *J. Semicond.*, 2021, 42(5), 050501. http://doi.org/10.1088/1674-4926/42/5/050501

SUPPORTING INFORMATION

Experimental section

Materials

SnO_2 colloid precursor (tin (IV) oxide, 15% in H_2O colloidal dispersion), zinc acetate dehydrate (99.5%), ethanolamine, and 2-methoxyethanol (99.8%) were purchased from Sigma Aldrich. N,N-dimethylformamide (DMF, >99.8%), dimethylsulfoxide (DMSO, >99.8%), chlorobenzene (99.9%), ethanolamine (>99.5%), 2-methxyethnol (>99.0%), molybdenum(VI) oxide (MoO_3, 99.998%) and lead bromide ($PbBr_2$, 99.999%) were purchased from Alfa Aesar. Cesium iodide (CsI, 99.99%) was purchased from Xi'an Polymer Light Technology Corp. (PLT). Lead iodide (PbI_2, 99.99%) and polymethyl methacrylate (PMMA) were purchased from TCI. Ethanol, isopropanol, acetone, and acetonitrile were purchased from Sinopharm Chemical Reagent Co., Ltd. Spiro-OMeTAD was purchased from 1 M Company Ltd. Lithium bis-(trifluoromethylsulfonyl) imide (Li-TFSI 99%) was purchased from Aladdin. 4-tertbutylpyridine (t-BP 97%) was purchased from Adamas Reagent.

Device fabrication

The ITO-coated glass substrate (Shenzhen Nan Bo Group, China) with a sheet resistance of 10 Ω sq^{-1} was ultrasonicated in detergent, deionized water, acetone, and isopropanol for 15 min before being dried at 60 °C. A thin SnO_2 layer was deposited by spin-coating dispersed SnO_2 colloid in deionized water (v/v 1 : 4.6) at the speed of 3000 rpm for 30 s, then annealed at 150 °C for 30 min. Then, the ZnO precursor solution was spin-coated onto substrates (4000 rpm for 30 s). The films were annealed at 200 °C in the air for 20 min. The ZnO precursor solution was prepared according to literature[1]. The $CsPbI_2Br$ precursor solution (comprised of 1.3 M CsI, 0.65 M PbI_2, 0.65 M $PbBr_2$ in 100 μL DMF and 900 μL DMSO) was spin-coated on the substrate at 3000 rpm for 40 s, chlorobenzene with different concentrations of PMMA (0, 0.01, 0.05, 0.5 mg/mL) was dropped onto the precursor film before after 20 s spin-coating and then continue spin-coating for 20 s. The prepared precursor film was then thermally annealed at 55 °C for 60 s and 240 °C for 10 min. For the deposition of hole transporting layer, spiro-OMeTAD (73.2 mg) was dissolved in 1 mL of chlorobenzene, then 28.8 μL of t-BP and 18.8 μL of Li-TFSI solution (520 mg Li-TFSI in 1 mL of acetonitrile) were added. The Spiro-OMeTAD solution was spin-coated onto the perovskite layer at 3000 rpm for 30 s. Finally, 6 nm MoO_3 and 75 nm silver (Ag) were thermally evaporated under vacuum (≈10^{-6} torr). A shadow mask was employed to make an effective device area of 0.1 cm^2. All device fabrication procedures were carried out in a N_2-purged glovebox (<0.1 ppm O_2 and H_2O).

Measurements and characterization

The current density voltage (*J–V*) characterizations were measured by a Keithley 2400 source measurement unit under simulated AM 1.5 irradiation (100 mW cm^{-2}) with a standard xenon-lamp-based solar simulator (XEC-300M2), which was calibrated with a monocrystalline silicon reference cell (Oriel P/N 91 150 V, with KG-5 visible color filter) calibrated by the National Renewable Energy Laboratory. A mask (well-defined area of 0.10 cm^2) was used for the measurements to ensure accurate measurement under ambient conditions. Around 40 devices were fabricated and measured independently under each experimental condition to check the reproducibility of the result and to obtain the statistical data of the photovoltaic parameters. The EQE measurements were performed on an ORIEL Intelligent Quantum Efficiency 200TM Measurement system established with a tunable light source. The SEM measurements were obtained via field-emission scanning electron microscope (FEI Apero). AFM images were acquired on a XE-7 scanning probe microscope in noncontact mode (Park systems, Korea). XRD patterns were attained on a Rigaku SmartLab X-ray diffractometer with Cu Kα radiation (0.154 nm). XPS measurements were performed on a Thermo ESCALAB 250 instrument with a monochromatized Al Kα X-ray source under vacuum. FTIR spectra were recorded as KBr pellets on a TENSOR 27 spectrometer (Bruker, Germany) at room temperature. The UV–Vis spectroscopy spectra were recorded on a UV–Vis–NIR 3600 spectrometer (Shimadzu, Japan). The steady-state PL spectra were acquired employing

Yanbo Shang and Zhimin Fang contributed equally to this work.
Correspondence to: L M Ding, ding@nanoctr.cn; S F Yang, sfyang@ustc.edu.cn
Received 24 FEBRUARY 2021.

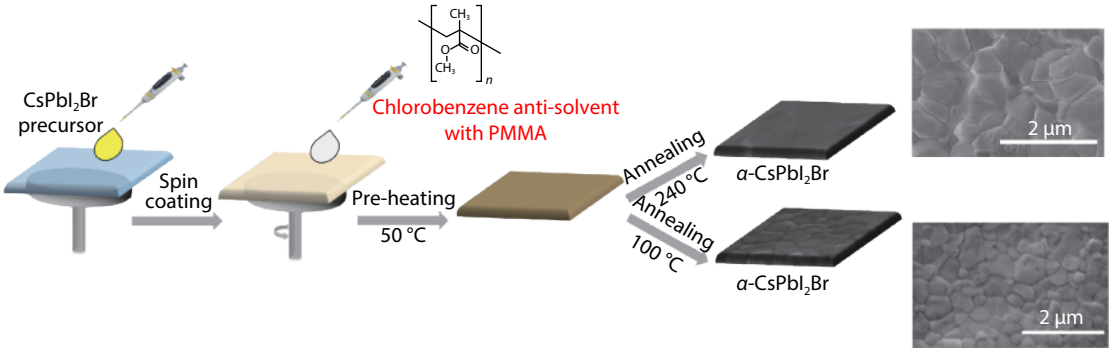

Fig. S1. Schematic illustration of the fabrication process of PMMA-incorporated $CsPbI_2Br$ perovskite films. The chemical structure of PMMA is shown at the top. A high temperature annealing (240 °C) or low temperature annealing (100 °C) is applied to the pre-heated film. The corresponding SEM images for the $CsPbI_2Br$ films with optimized PMMA concentration (0.05 mg/mL) are also shown.

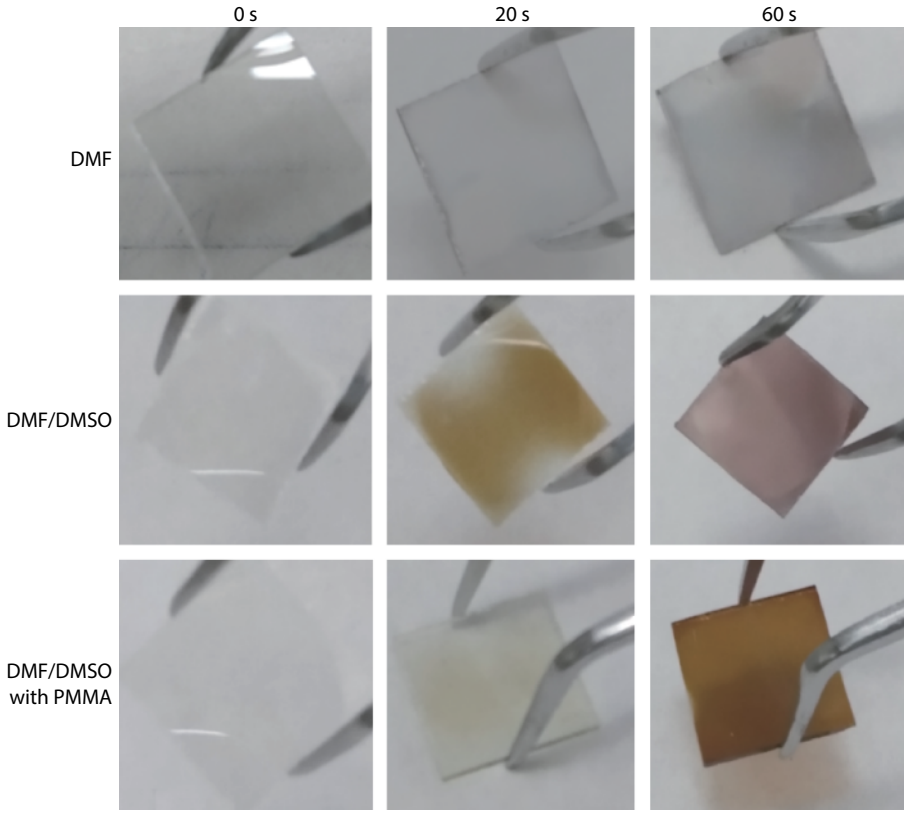

Fig. S2. Photos of the $CsPbI_2Br$ perovskite films prepared using different solvent under an annealing temperature of 50 °C.

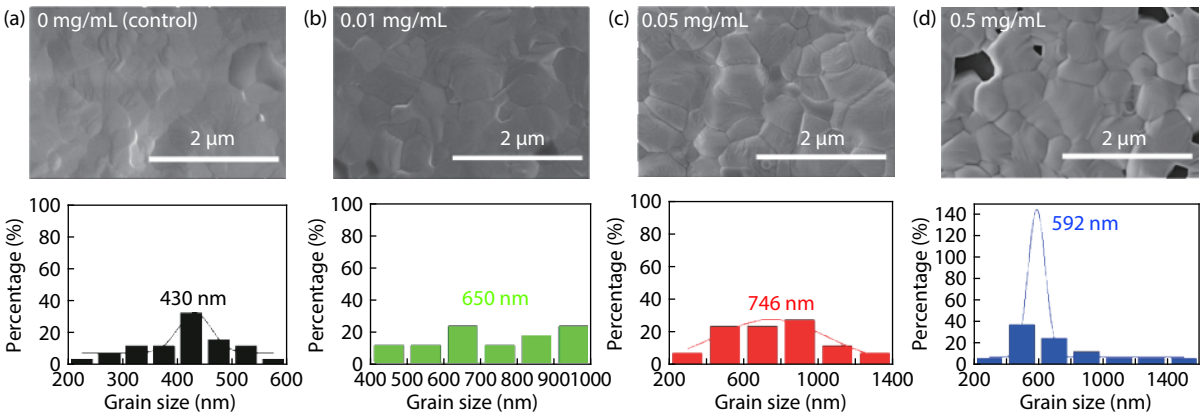

Fig. S3. Surface topographic SEM images and corresponding grain size distribution of $CsPbI_2Br$ films prepared using different concentration of PMMA.

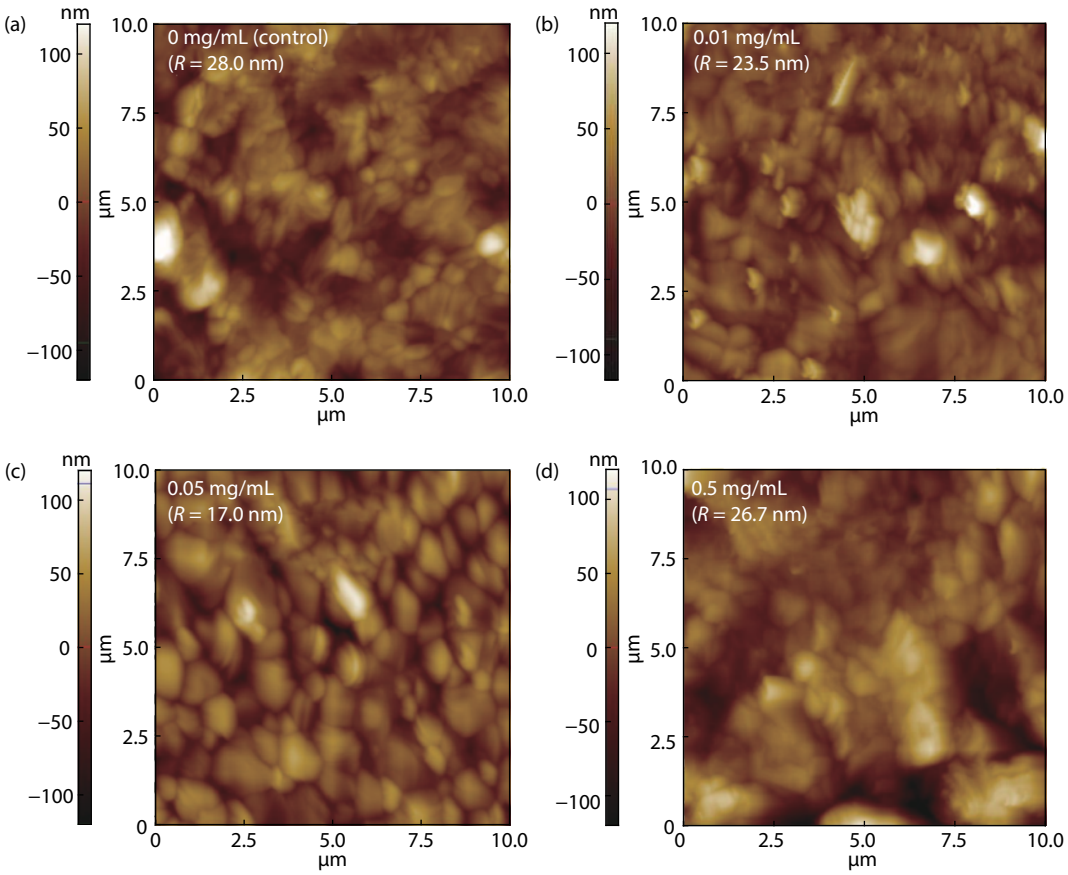

Fig. S4. AFM images of high-temperature annealed $CsPbI_2Br$ films prepared using different concentration of PMMA. (a) 0 mg/mL. (b) 0.01 mg/mL. (c) 0.05 mg/mL. (d) 0.5 mg/mL.

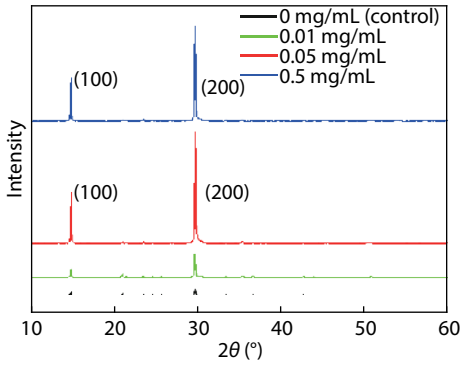

Fig. S5. X-ray diffraction (XRD) patterns of $CsPbI_2Br$ films prepared using different concentration of PMMA.

an Edinburgh Instruments FLS920 fluorescence spectrometer with an excitation wavelength of 460 nm. EIS measurements were performed in the dark using an electrochemical workstation (Autolab 320, Metrohm, Switzerland) with a frequency range from 1 Hz to 1 MHz under 1.0 V. Alternating current (20 mV) perturbation was applied with a frequency from 1 MHz to 1 Hz. The obtained impedance spectra were fitted with Z-View software (v2.8b, Scribner Associates).

The $CsPbI_2$ film without PMMA shows a compact morphology with fuzzy grain boundaries, and the average grain size is about 430 nm. Interestingly, upon incorporating PMMA, the grain boundaries become much clearer, and the average grain size increases obviously. Under the optimized concentration of PMMA in chlorobenzene (0.05 mg/mL), the $CsPbI_2Br$ film looks homogeneous and pinhole-free, and the average grain size increases to 746 nm, which is much larger than that of the film with 0.01 mg/mL PMMA (650 nm). Nevertheless, when PMMA concentration is increased to 0.5 mg/mL, the grain size becomes smaller, and obvious holes appear, indicating deteriorated film quality.

Space charge limited current (SCLC) method

We studied the trap-state density in $CsPbI_2Br$ by using space charge limited current (SCLC) method based on an electron-only device with a structure of ITO/SnO_2/ZnO/perovskite/PCBM/Ag[2]. The trap-state density (n_t) can be calculated by equation:

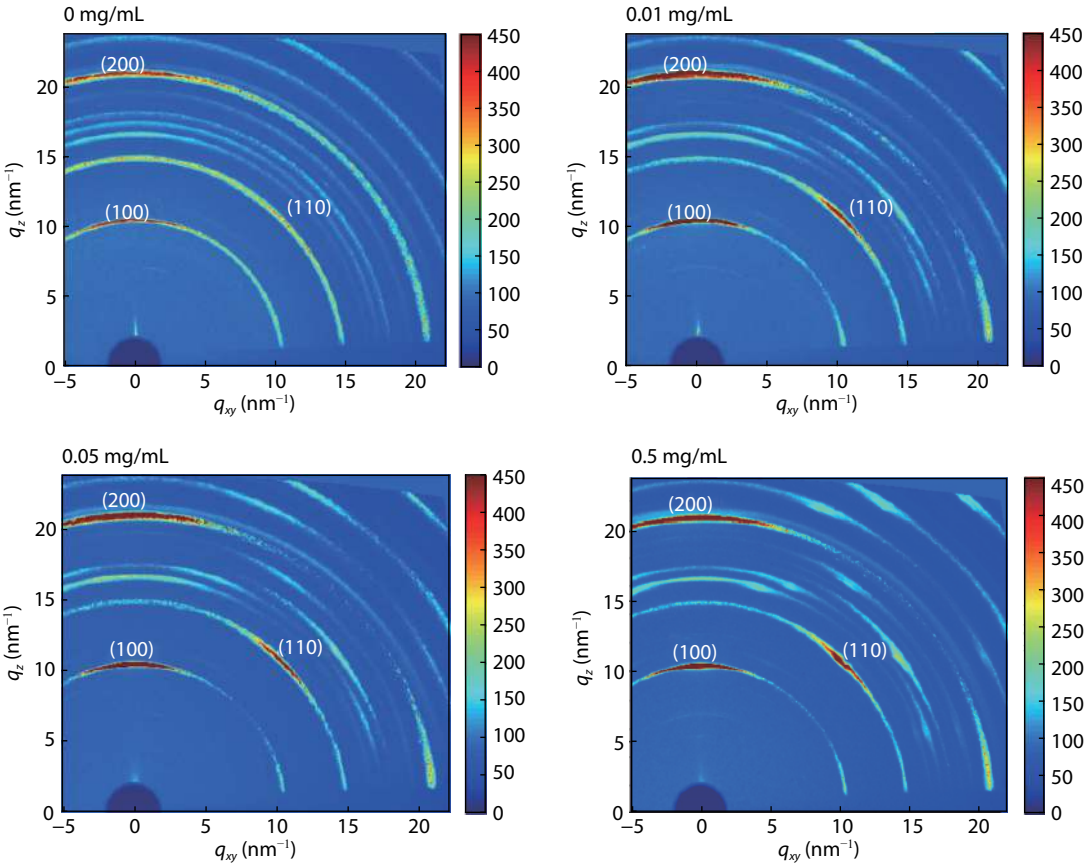

Fig. S6. 2D-GIXRD patterns of the perovskite films prepared using different concentration of PMMA.

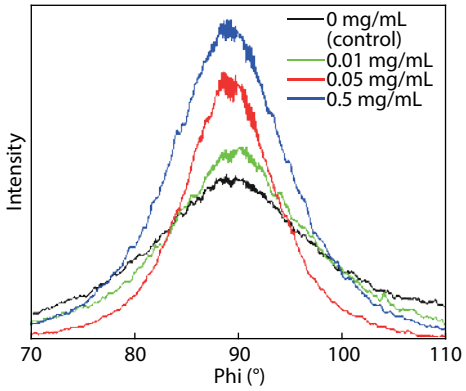

Fig. S7. The azimuthally integrated intensity profiles for the perovskite films.

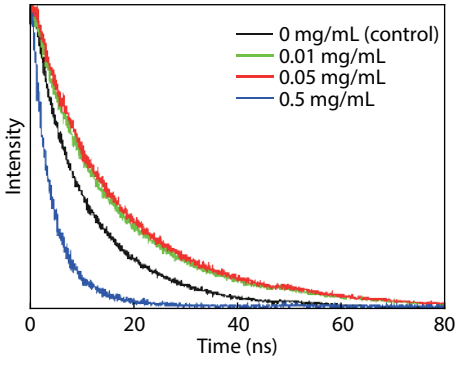

Fig. S8. TRPL spectra of $CsPbI_2Br$ films prepared using different concentration of PMMA on glass substrate.

Table 1. Time constants in TRPL determined by bi-exponential fittings measured on $CsPbI_2Br$ films with and without PMMA.

Concentration (mg/mL)	A_1	τ_1 (ns)	A_2	τ_2 (ns)	t (ns)
0	0.418	4.247	0.625	7.582	6.68
0.01	0.636	5.284	0.378	12.95	9.83
0.05	0.681	5.728	0.355	13.97	10.34
1	0.697	1.828	0.08	5.30	2.69

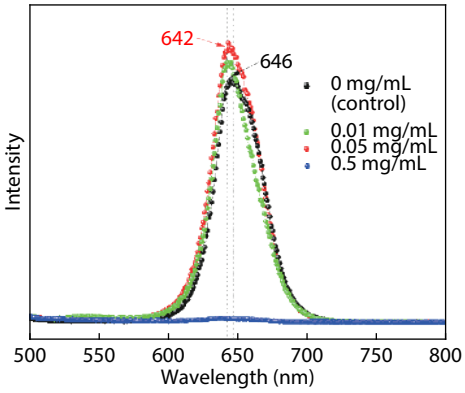

Fig. S9. Steady-state PL spectra of $CsPbI_2Br$ films prepared using different concentration of PMMA on glass substrate.

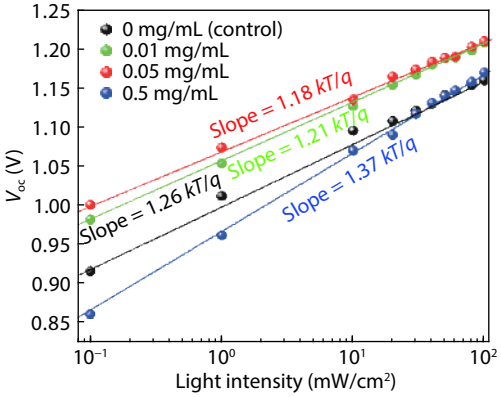

Fig. S10. Changing of V_{oc} with the light intensity for $CsPbI_2Br$ cells prepared using different concentration of PMMA.

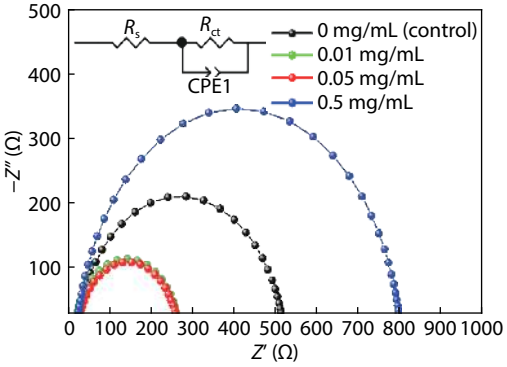

Fig. S11. Nyquist plots of the impedance spectra (measured in the dark under a reverse potential of 1.0 V) for $CsPbI_2Br$ cells prepared using different concentration of PMMA.

$$n_t = \frac{2\varepsilon\varepsilon_0}{eL^2} \times V_{TFL}$$

where ε_0 is the vacuum permittivity, ε is the relative dielectric constant of $CsPbI_2Br$[3], e is the elementary charge of the electron, and L is the thickness of perovskite film, the trap-filled limit voltage (V_{TFL}) is the bias voltage at the kink point.

The excitation source was a 543 nm picosecond laser pulse which was filtered from a super continuum generation. The TRPL spectrum can be fitted by a single-exponential decay function as shown in Eq. (S1):

$$f(t) = \sum A_i \cdot \exp(-t/\tau_i) + B, \quad (1)$$

Table 2. Parameters employed for the fitting of the impedance spectra.

PMMA concentration (mg/mL)	R_s (Ω cm^2)	R_{ct} (Ω cm^2)	CPE (10^{-7} F/cm^2)
0	1.71	50.2	2.31
0.01	1.39	25.4	1.09
0.05	1.27	24.3	2.85
0.5	1.95	77.9	1.46

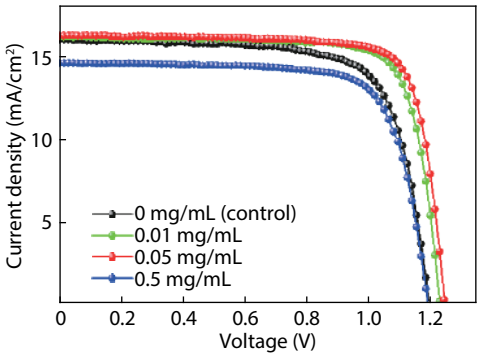

Fig. S12. *J*–*V* curves for $CsPbI_2Br$ cells prepared using different concentration of PMMA (annealing temperature: 240 °C).

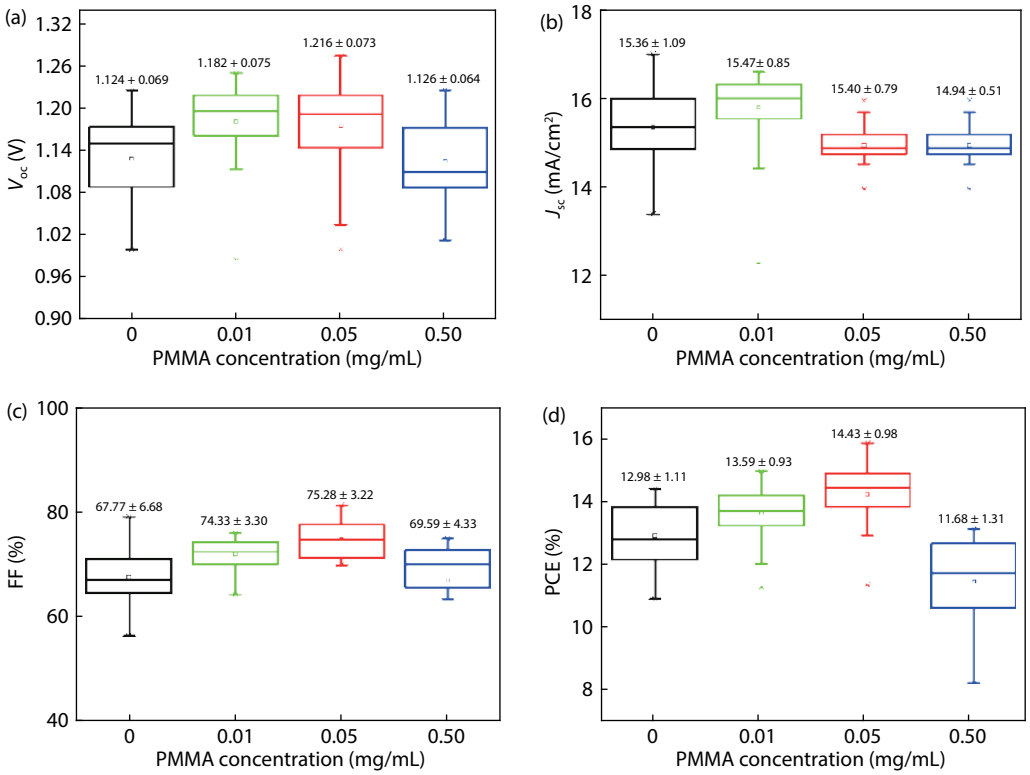

Fig. S13. Box plots of (a) V_{oc}, (b) J_{sc}, (c) FF, and (d) PCE for the $CsPbI_2Br$ cells prepared using different concentration of PMMA.

where *A*, τ, and *B* are the decay amplitude, the decay lifetime, and a constant for the baseline offset, respectively. The fast decay (τ_1) component is ascribed to the surface recombination, while the slow decay (τ_2) component is attributed the recombination occurring in the bulk of the perovskite[4].

To get direct insight into the charge recombination kinetics within the device, we next investigated the dependence of V_{oc} on the incident light intensity, which can be fitted according to the equation:

$$V_{oc} = \frac{kT}{e}\ln(I) + \text{constant},$$

where ε is the ideal factor related to the dominant recombination mechanism in the device, *k* is the Boltzmann constant, *T* is the absolute temperature, *e* refers to the elementary charge. In particular, an ideal factor (ε) larger than 1 indicates the presence of additional trap-assisted Shockley-Read-Hall (SRH) recombination, and decrease in the slope indicates a suppression of the monomolecular SRH recombination, leading to improved device performance. For the cells prepared using 0.05 mg/mL PMMA, the ε value decreases from 1.26 (control) to 1.18. This confirms the suppression of trap-assisted carrier recombination, which is consistent with the trap

Table 3. Photovoltaic parameters for $CsPbI_2Br$ cells prepared using different concentration of PMMA.

Concentration(mg/mL)		V_{oc} (V)	J_{sc} (mA/cm^2)	FF (%)	PCE (%)	R_s[b] (Ω cm^2)	R_{sh}[b] (Ω cm^2)
0	Average[a]	1.124 ± 0.069	15.36 ± 1.09	67.77 ± 6.68	12.98 ± 1.11	12.7	1157.9
	Best	1.227	16.01	73.38	14.42	9.7	2694.4
0.01	Average[a]	1.182 ± 0.075	15.47 ± 0.85	74.33 ± 3.30	13.59 ± 0.93	10.9	2315.8
	Best	1.235	16.11	75.36	14.99	7.8	3532.0
0.05	Average[a]	1.216 ± 0.073	15.56 ± 0.79	75.28 ± 3.22	14.43 ± 0.98	8.8	3977.2
	Best	1.252	16.23	78.13	15.88	5.9	3754.6
0.5	Average[a]	1.120 ± 0.064	14.94 ± 0.51	69.59 ± 4.33	11.68 ± 1.31	12.9	1770.8
	Best	1.174	14.93	75.76	13.28	8.6	2215.1

[a]Calculated from 42 cells; [b]R_s and R_{sh} were given by the PCE measurement system.

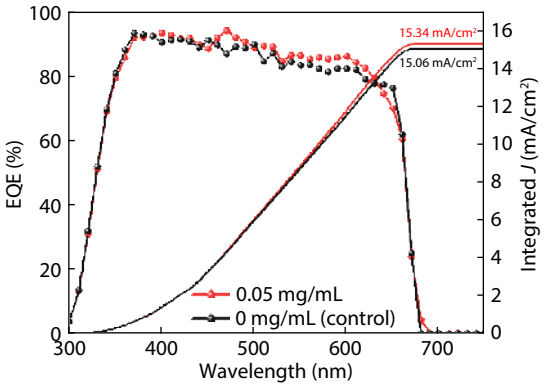

Fig. S14. EQE spectra for the cells prepared using 0 mg/mL (Control) and 0.05 mg/mL PMMA.

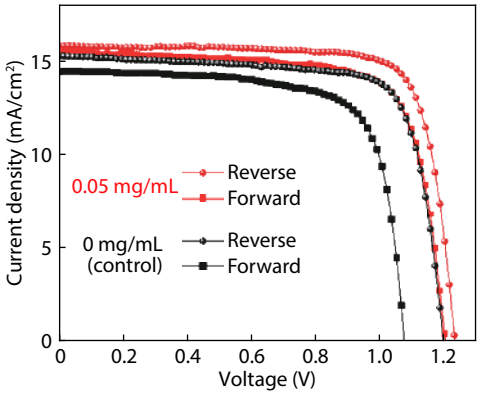

Fig. S15. *J*–*V* curves obtained from different scan directions for the cells prepared using 0 mg/mL (Control) and 0.05 mg/mL PMMA.

Table 4. Performance parameters of the champion cells obtained from different scan directions with a scan rate of 0.1 V/s.

Devices	Scandirection	V_{oc} (V)	J_{sc} (mA/cm^2)	FF (%)	PCE (%)	Hysteresis index[a] (%)
Control 240 °C	Reverse	1.215	15.33	75.88	14.13	9.1
	Forward	1.050	14.52	74.84	12.84	
PMMA[b] 240 °C	Reverse	1.224	15.85	78.21	15.18	6.5
	Forward	1.212	15.54	75.39	14.20	
Control 100 °C	Reverse	1.142	15.01	74.48	12.76	15.8
	Forward	1.051	14.47	70.69	10.74	
PMMA[b] 100 °C	Reverse	1.170	15.64	75.38	13.78	9.7
	Forward	1.160	14.65	73.15	12.43	

[a]Hysteresis index = [PCE(reverse) – PCE(forward)]/PCE(reverse).[b]0.05 mg/mL PMMA in chlorobenzene antisolvent.

passivation deduced from the PL study.

The impedance spectra were fitted with one R-CPE arcs (Fig. S11). R_s is determined by the starting point at the real part of the Nyquist plot. The R_{ct} (charge transfer resistance) is related to the charge transfer dynamics of devices, CPE is the non-ideal chemical capacitances[5].

According to the comparison of the Nyquist plots and the corresponding fitted curves of devices with and without

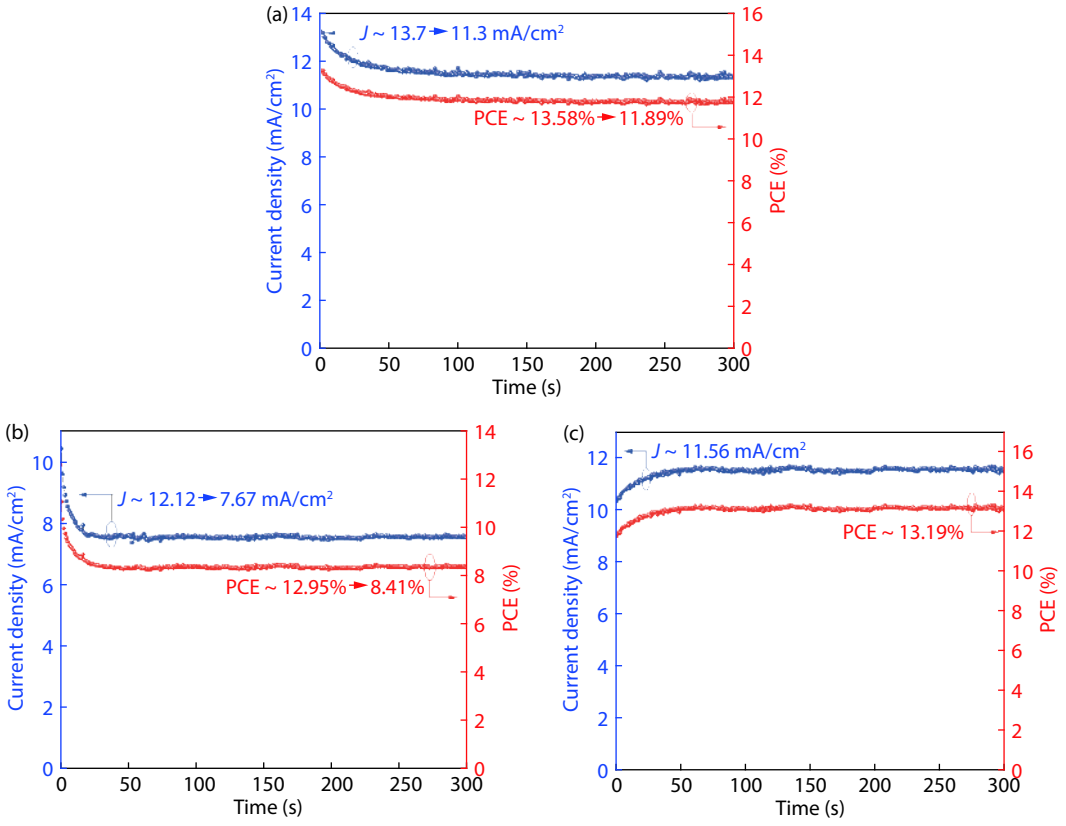

Fig. S16. (a) Stabilized power output (SPO) of the high-temperature processed cell without PMMA. (b) SPO of the low-temperature processed cell without PMMA and (c) with 0.05 mg/mL PMMA.

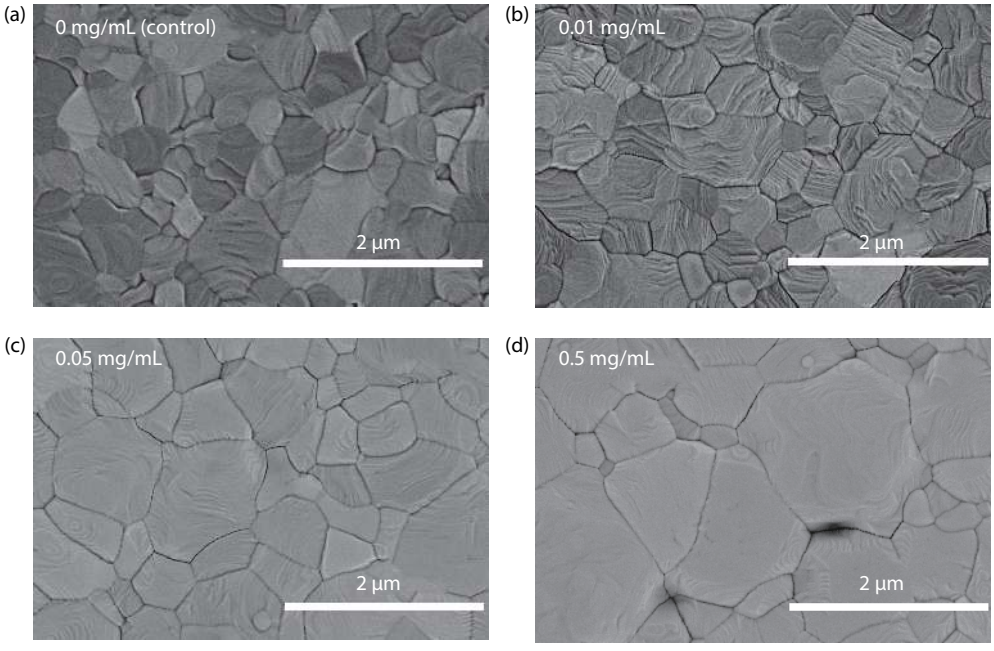

Fig. S17. SEM images at BSE mode for the high temperature processed $CsPbI_2Br$ films prepared using different concentration of PMMA.

PMMA measured in the dark under a reverse potential of 1.0 V (near the open circuit potential) shown in Fig. S11, the R_s (series resistance) value exhibits a slight decrease from 1.71 to 1.27 Ω cm^2, whereas the R_{ct} (charge transfer resistance) value decreases dramatically from 50.2 to 24.3 Ω cm^2 after PMMA incorporation (Table S2), indicating facilitated interfacial charge transport. This is likely due to the improved smoothness of $CsPbI_2Br$ film as discussed above.

As shown in Fig. S21, for the $CsPbI_2Br$ film without PMMA, Pb 4f 7/2 and Pb 4f 5/2 peaks located at 143.18 and 138.28 eV, respectively. The peaks shift to lower binding energies by ~0.2 eV after PMMA incorporation. This is due to the in-

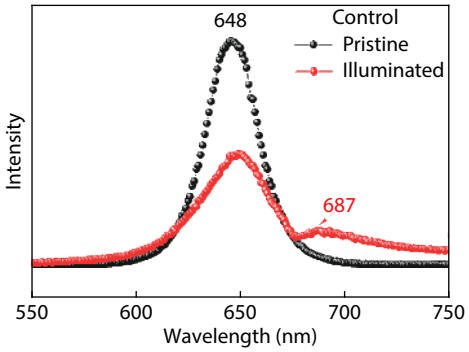

Fig. S18. Steady-state PL spectra of the $CsPbI_2Br$ film without PMMA before and after illumination.

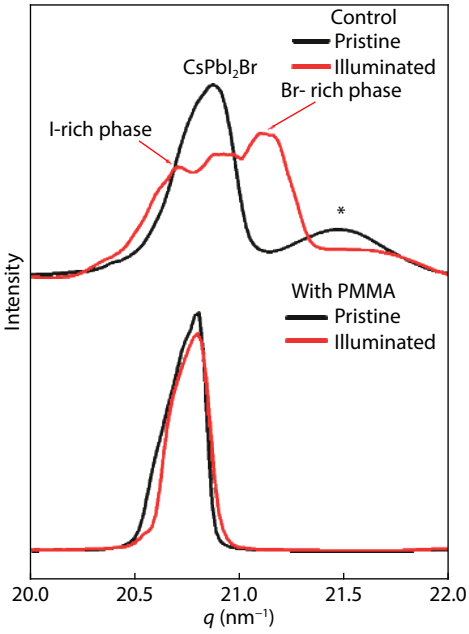

Fig. S19. The radial integrated intensity profiles of the $CsPbI_2Br$ film without and with 0.05 mg/mL PMMA before and after illumination. The asterisk denotes ITO substrate.

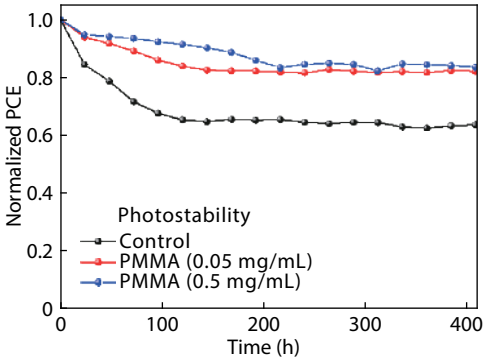

Fig. S20. Normalized PCE of the $CsPbI_2Br$ cells prepared using different concentration of PMMA under continuous 1 sun equivalent illumination.

creased electron cloud density around Pb^{2+} ions, resulted from the donation of the lone electron pair on the oxygen (O) atom of the C=O group within PMMA to the empty 6p orbital of Pb^{2+} *via* coordination bonding.

We used Fourier transform infrared spectroscopy (FTIR) to study the influence of Pb^{2+} on the vibrational signal of the C=O groups. Interestingly, after blending PMMA with PbI_2 or $PbBr_2$, the vibrational signal of the C=O group obviously shifts negatively from 1741.3 to 1731.9 cm^{-1} (PbI_2) and 1727.8 cm^{-1} ($PbBr_2$) (Fig. S22). Such a negative shift of the C=O vibration peak indicates the weakened C=O bond strength, due to its coordination interaction with Pb^{2+} within

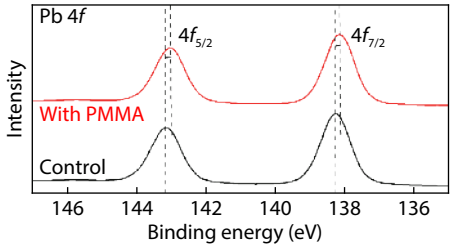

Fig. S21. Pb 4f XPS spectra of $CsPbI_2Br$ films with and without PMMA.

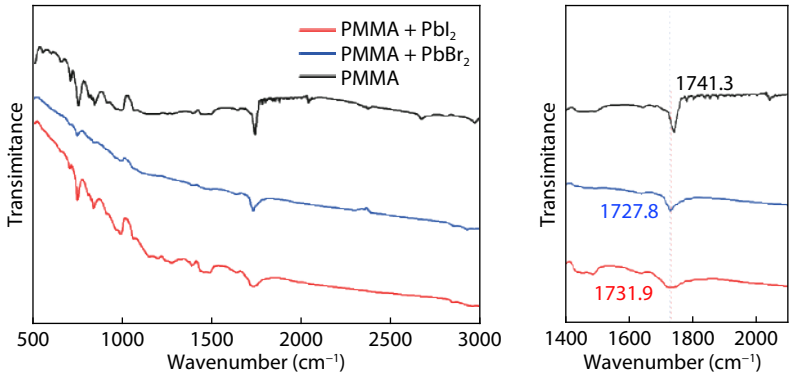

Fig. S22. FTIR spectra for PbI_2·PMMA (molar ratio: 1 : 1), $PbBr_2$·PMMA (molar ratio: 1 : 1), and pristine PMMA.

PbI_2 or $PbBr_2$.

References

[1] Shen E, Chen J, Tian Y, et al. Interfacial energy level tuning for efficient and thermostable $CsPbI_2Br$ perovskite solar cells. Adv Sci, 2020, 7, 1901952

[2] Li B, Zhen J, Wan Y, et al. Anchoring fullerene onto perovskite film via grafting pyridine toward enhanced electron transport in high-efficiency solar cells. ACS Appl Mater Interfaces, 2018, 10, 32471

[3] Fu S, Zhang W, Li X, et al. Dual-protection strategy for high-efficiency and stable $CsPbI_2Br$ inorganic perovskite solar cells. ACS Energy Lett, 2020, 5, 676

[4] Chen P, Bai Y, Wang S, et al. In situ growth of 2D perovskite capping layer for stable and efficient perovskite solar cells. Adv Funct Mater, 2018, 28, 1706923

[5] Zhou W, Li D, Xiao Z, et al. Zwitterion coordination induced highly orientational order of $CH_3NH_3PbI_3$ perovskite film delivers a high open circuit voltage exceeding 1.2 V. Adv Funct Mater, 2019, 29, 1901026